Superconductivity and Field-Induced Magnetism in $SrFe_{1.75}Co_{0.25}As_2$

R. Khasanov,[1,*] A. Maisuradze,[1] H. Maeter,[2] A. Kwadrin,[2] H. Luetkens,[1] A. Amato,[1] W. Schnelle,[3] H. Rosner,[3]
A. Leithe-Jasper,[3] and H.-H. Klauss[2]

[1]*Laboratory for Muon Spin Spectroscopy, Paul Scherrer Institut, CH-5232 Villigen PSI, Switzerland*
[2]*IFP, Technische Universität Dresden, 01069 Dresden, Germany*
[3]*Max-Planck-Institut für Chemische Physik fester Stoffe, Nöthnitzer Str. 40, 01187 Dresden, Germany*

Using muon-spin rotation, we studied the in-plane (λ_{ab}) and the out of plane (λ_c) magnetic field penetration depth in $SrFe_{1.75}Co_{0.25}As_2$ ($T_c \simeq 13.3$ K). The penetration depth anisotropy $\gamma_\lambda = \lambda_c/\lambda_{ab}$ increases from $\gamma_\lambda \simeq 2.1$ at T_c to 2.7 at 1.6 K. The mean internal field in the superconducting state increases with decreasing temperature, just opposite to the diamagnetic response seen in magnetization experiments. This unusual behavior suggests that the external field induces a magnetic order which is maintained throughout the whole sample volume.

The discovery of Fe-based high-temperature superconductors (HTS) with critical temperatures exceeding 50 K has triggered a surge of theoretical and experimental studies. Similar to cuprates, Fe-based HTS are characterized by a layered structure and by a superconducting state emerging upon doping from the parent compound exhibiting long-range antiferromagnetic (AFM) order. On the other hand, the metallicity of the parent compounds, as well as the occurrence of superconductivity on a few disconnected pieces on the Fermi surface clearly distinguish them from cuprate HTS. A fundamental question is whether the mechanism(s) leading to the occurrence of the superconducting and magnetic ground states in both families share common origin. The answer can be found by monitoring carefully the emergence of these ground states as a function of chemical doping, applied magnetic field or external pressure.

In lightly doped cuprate HTS, the static stripelike magnetism coexists with superconductivity on a nanometer scale [1–4]. In Fe-based HTS, like $LnO_{1-x}F_xFeAs$ (Ln = La, Ce, etc.) and $(Sr, Ba)_{1-x}K_xFe_2As_2$ the majority of the reported phase diagram studies demonstrate, in contrast, either the occurrence of an abrupt first-order like change, with a full suppression of the AFM order, at the doping where superconductivity emerges [5,6], or point to a microscopic separation of magnetism and superconductivity [7,8]. To date, a microscopic coexistence of both states is solely reported for the system $SmFeAsO_{1-x}F_x$ [9,10].

The subtle balance between superconductivity and magnetism in cuprate HTS is strongly affected by the magnetic field. Field-induced or enhanced static magnetic order are detected in various underdoped cuprates. In electron doped $Pr_{2-x}Ce_xCuO_{4-y}$ [11] and $Pr_{1-x}LaCe_xCuO_{4-y}$ [12], e.g., even a magnetic field as low as 10 mT is sufficient to enhance the weak AFM ordering over the entire sample volume. For Fe-based HTS we are aware of only two reports pointing to a possible enhancement of magnetism

by applied magnetic field [13,14]. Here, we report on muon-spin rotation (μSR) studies of a single crystalline sample of $SrFe_{1.75}Co_{0.25}As_2$. In zero external field, superconductivity coexists with dilute Fe spins which are static on the μSR time scale. In the superconducting state, the applied field leads to the appearance of an additional source of local magnetic field, maintained throughout the whole volume of the sample, thus pointing to the field-induced ordering of the Fe moments.

The $SrFe_{1.75}Co_{0.25}As_2$ (SFCA) single-crystalline samples were synthesized as described in [15]. The zero-field-cooled (ZFC) and field-cooled (FC) DC susceptibility (χ) measurements confirm bulk superconductivity (see Fig. 1 and Ref. [15]). The transition temperature (T_c) of 13.3(1) K is consistent with the overdoped composition of the sample [16]. The true FC Meissner effect is very small, suggesting that pinning in SFCA is relatively strong. The
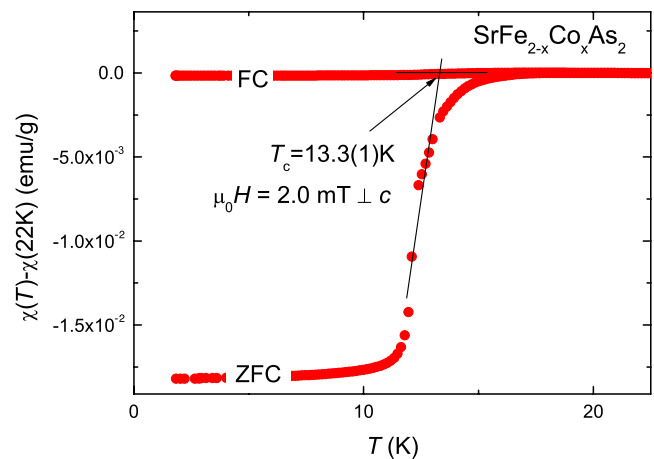

FIG. 1 (color online). ZFC and FC magnetic susceptibility (χ) of $SrFe_{1.75}Co_{0.25}As_2$ (the paramagnetic contribution measured at $T = 22$ K is subtracted). T_c is obtained as the intersect of linearly extrapolated $\chi_{ZFC}(T)$ with the zero line.

ZFC shielding is ∼100%. All crystals used in our study were taken from the same growth batch and show very similar $\chi(T)$ dependences.

The μSR experiments were carried out at the πM3 beam line (Paul Scherrer Institute, Switzerland). Three SFCA single crystals with an approximate size of $2.5 \times 2.0 \times 0.1$ mm^3 were used. The zero-field (ZF), transverse-field (TF), and longitudinal-field (LF) μSR experiments were performed at temperatures ranging from 1.5 to 150 K. In two sets of TF measurements the external magnetic field $\mu_0 H = 10$ mT was applied parallel and perpendicular to the c axis, and always perpendicular to the muon-spin polarization. The typical counting statistics were $\sim 1.5 \cdot 10^7$ positron events for each particular data point.

In ZF, the muon-spin polarization is relaxed by magnetic moments of electronic and nuclear origin. As shown in Fig. 2(a), the ZF μSR signal is the same down to $T \simeq 5$ K, while at lower temperatures an additional fast relaxing component starts to develop. The solid lines in Fig. 2(a) correspond to the fit by:

$$A^{ZF}(t) = A_1 \exp(-\Lambda_1 t) + A_2 \exp(-\Lambda_2 t). \quad (1)$$

Here $A_1(A_2)$ and $\Lambda_1(\Lambda_2)$ are the initial asymmetry and the exponential depolarization rate of the slow (fast) relaxing component, respectively. The temperature dependence of A_1 normalized to the total ZF asymmetry $A_1 + A_2$, which was kept fixed during the fit, is shown in the inset. The fit reveals that Λ_1 is temperature independent which is also clearly seen from the raw data as a parallel shift of $A^{ZF}(t)$ at $t \gtrsim 0.2$ μs with decreasing temperature. Measurements in LF geometry indicate that the exponential character of the muon-spin relaxation is due to randomly oriented local magnetic fields, which are static on the μSR time scale. Such behavior is consistent with dilute Fe moments as observed recently for another representative of Fe-based HTS FeSe$_{0.85}$ [17].

In the TF geometry muons measure the magnetic field distribution [$P(B)$] inside the sample. For the superconductor in the vortex state, $P(B)$ is uniquely determined by the magnetic penetration depth λ and the coherence length ξ [18]. A few representative $P(B)$ distributions, obtained after Fourier transformation of TF μSR time-spectra, are presented in Figs. 2(b) and 2(c). In the normal state, a symmetric line at the position of the external magnetic field with a broadening arising from the nuclear and electronic magnetic moments is seen. Below T_c, the field distribution is broadened and asymmetric which is characteristics of the inhomogeneous field distribution within the flux line lattice (FLL).

In an orthogonal reference frame (x, y, z) with $H \parallel z$ (z is one of the principal axes a, b, or c) the spatial magnetic field distribution within a FLL of an anisotropic superconductor is [18]:

$$B(\mathbf{r}) = \langle B \rangle \sum_{\mathbf{G}} \exp(-i\mathbf{G} \cdot \mathbf{r}) B_{\mathbf{G}}(\lambda_x, \lambda_y, \xi_x, \xi_y). \quad (2)$$

$\mathbf{G}$ is the reciprocal lattice vector, $\langle B \rangle$ is the average magnetic field inside the superconductor, $\mathbf{r}$ is the vector coordinate in a plane perpendicular to the applied field, and the Fourier components $B_{\mathbf{G}}$, obtained within the framework of the Ginzburg-Landau (GL) model, are [18]:

$$B_{\mathbf{G}} = \frac{\Phi_0}{S}(1 - b^4) \frac{uK_1(u)}{\lambda_x^2 G_y^2 + \lambda_y^2 G_x^2}. \quad (3)$$

Here, Φ_0 is the magnetic flux quantum, $S = \Phi_0/\langle B \rangle$ is the FLL unit cell area, $b = \langle B \rangle/B_{c2}$ (B_{c2} is the second critical field), $K_1(u)$ is the modified Bessel function, and $u^2 = 2(\xi_x^2 G_x^2 + \xi_y^2 G_y^2)(1 + b^4)[1 - 2b(1 - b)^2]$. The reciprocal lattice corresponding to the hexagonal FLL is: $\mathbf{G}_{m,n} = (2\pi/S)(ym, (n - m/2)x)$, where $x = (2S\lambda_x/\sqrt{3}\lambda_y)^{1/2}$, $y = (\sqrt{3}S\lambda_y/2\lambda_x)^{1/2}$, and m and n are the integer numbers [19]. Note that in the uniaxial case ($\lambda_x = \lambda_y$), Eq. (3) converts into the standard GL equation for an isotropic superconductor [18].

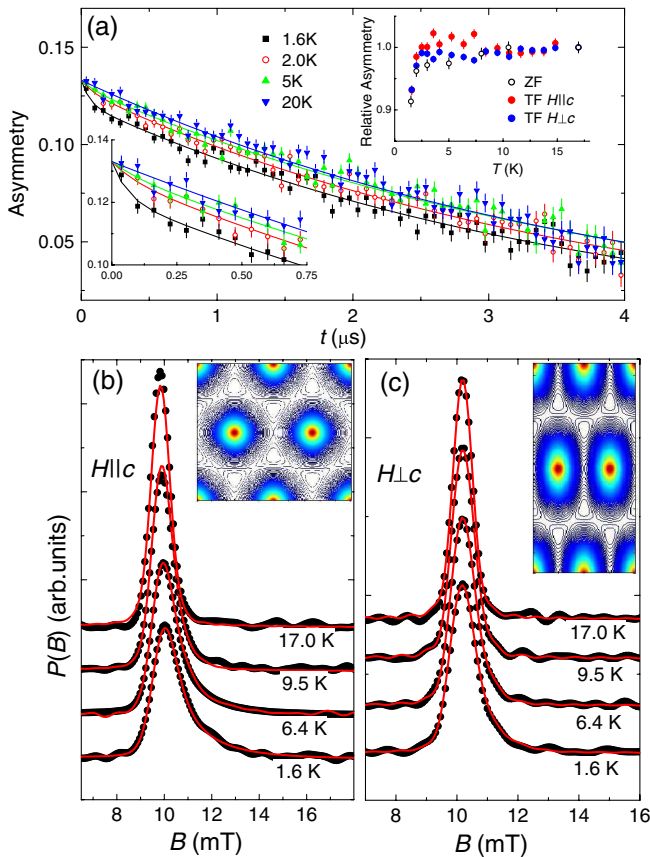The TF μSR time spectra were fitted to a theoretical asymmetry function $A^{TF}(t)$ by assuming the internal field

FIG. 2 (color online). (a) ZF μSR time spectra of SrFe$_{1.75}$Co$_{0.25}$As$_2$. The lines are fits by Eq. (1). Insets show the temperature dependences of normalized asymmetries and the extended part of the ZF μSR data for $t \le 0.75$ μs. (b), (c) The magnetic field distributions $P(B)$ obtained in the $H \parallel c$ and $H \perp c$ set of TF μSR experiments. The lines are the fits by Eq. (4). The insets represent the contour plots of field variation.

distribution $P_{id}(B)$ obtained from Eq. (2) and accounting for the FLL disorder and the electronic moment contributions (see the ZF discussion above) by convoluting $P_{id}(B)$ with Gaussian and Lorenzian functions:

$$A^{TF}(t) = Ae^{i\phi}e^{-\sigma_g^2 t^2/2 - \Lambda t} \int P_{id}(B)e^{i\gamma_\mu Bt} dB. \quad (4)$$

Here A and ϕ are the initial asymmetry and the phase of the muon spin ensemble, σ_g accounts for the FLL disorder [20], and Λ relates to the electronic moment contribution and is assumed to be temperature independent (in analogy with Λ_1 in ZF experiments). During the analysis we first fit the data measured in $H \parallel c$ orientation which, considering $\lambda_a = \lambda_b$, allows us to obtain the in-plane magnetic penetration depth λ_{ab}. Note that at such a low field as $\mu_0 H = 10$ mT, $P(B)$ is independent on ξ [20,21]. The $H \perp c$ set of data was further analyzed by assuming in Eq. (3) $\lambda_x = \lambda_{ab}$, which was fixed to the value obtained from the fit of $H \parallel c$ data, and $\lambda_y = \lambda_c$. The resulting fitted curves are shown in Figs. 2(b) and 2(c) by red (light gray) lines. The field distributions obtained by Eq. (2) are shown in the insets.

The temperature dependences of the initial asymmetries are shown in the inset of Fig. 2(a). Both, $A^{\parallel c}(T)$ and $A^{\perp c}(T)$ are almost constant down to $T \simeq 3$ K and decrease by $\sim 10\%$ at $T = 1.6$ K just resembling the temperature behavior of the slow relaxing component A_1 observed in ZF measurements. This suggests that the fast relaxing component, seen in ZF μSR experiments, appears from areas where magnetism sets in. The superconductivity in such regions may either coexist with magnetism on a nanometer scale [10], or become suppressed due to enhanced magnetic order [8,22].

The dependence of λ_{ab}^{-2} and λ_c^{-2} on temperature is shown in Fig. 3(a). The experimental data were analyzed within the framework of the phenomenological α model by assuming two independent contributions to λ^{-2} [23]:

$$\frac{\lambda^{-2}(T)}{\lambda^{-2}(0)} = \omega \frac{\lambda^{-2}(T, \Delta_{0,1})}{\lambda^{-2}(0, \Delta_{0,1})} + (1 - \omega) \frac{\lambda^{-2}(T, \Delta_{0,2})}{\lambda^{-2}(0, \Delta_{0,2})}. \quad (5)$$

In this model, each superconducting gap, $\Delta_1(T)$ and $\Delta_2(T)$, has a similar temperature dependence given by $\Delta_i(T) = \Delta_{i,0} \tanh\{1.82[1.018(T_c/T - 1)]^{0.51}\}$, Ref. [23], but different zero-temperature values ($\Delta_{0,i}$, $i = 1, 2$). In our analysis both the large and the small gap were assumed to be of s-wave symmetry. The parameter ω accounts for the relative contribution of the larger gap to λ^{-2} and $\lambda^{-2}(0)$ is the penetration depth at $T = 0$. Each component $\lambda^{-2}(T, \Delta_{0,i})/\lambda^{-2}(0, \Delta_{0,i})$ is calculated within the local (London) approximation by assuming the sample to be in the "clean" ($\xi \ll l$, l is the mean free path) and the "dirty" ($\xi \sim l$) limit [24]. During the fit, both $\lambda_{ab}(T)$ and $\lambda_c(T)$ were described by the same small and large gaps ($\Delta_{1(2),ab} = \Delta_{1(2),c}$), but different weighting factors ($\omega_{ab} \neq \omega_c$). The results of the fit are summarized in Fig. 3(a) and Table I. The temperature dependence of the anisotropy parameter $\gamma_\lambda = \lambda_c/\lambda_{ab}$ is shown in the inset.
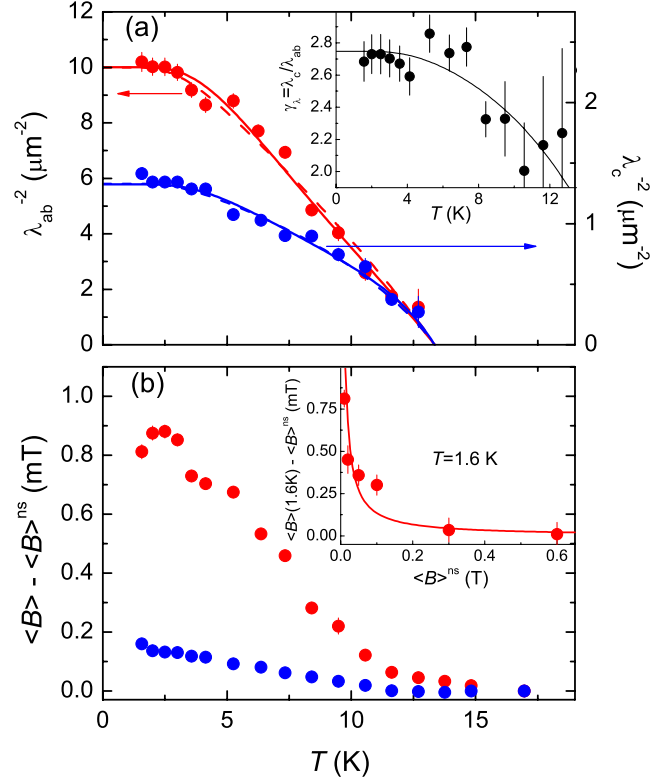

FIG. 3 (color online).   (a) Dependence of λ_{ab}^{-2} and λ_c^{-2} on temperature of SrFe$_{1.75}$Co$_{0.25}$As$_2$. The solid and the dashed lines are the fits by Eq. (5) within the clean and the dirty limit with the parameters summarized in Table I. The inset shows the temperature dependence of the penetration depth anisotropy $\gamma_\lambda = \lambda_c/\lambda_{ab}$. (b) Temperature dependence of $\langle B \rangle - \langle B \rangle^{ns}$ obtained in the $H \parallel c$ [red (light gray) symbols] and $H \perp c$ [blue (dark gray) symbols] set of experiments. The inset shows the dependence of $\langle B \rangle (1.6 \text{ K}) - \langle B \rangle^{ns}$ on $\langle B \rangle^{ns}$ in $H \parallel c$ orientation.

Four important results are deduced from this analysis: (i) The contribution of the large gap to $\lambda_{ab}^{-2}(T)$ is small in comparison with that for Ba$_{1-x}$K$_x$Fe$_2$As$_2$ [22]. This may be explained by the fact that the electron doping due to Co substitution reduces the size of the Fermi surface pockets at the Brillouin zone center (where the large gap opens), but leads to substantial enhancement of the pockets at the zone corner (where the small gap develops) [25,26]. (ii) γ_λ increases from $\gamma_\lambda \simeq 2.1$ at T_c to 2.7 at 1.6 K in agreement with the general trend obtained for various Fe-based HTS [22,27]. The different temperature dependences of λ_{ab}^{-2} and λ_c^{-2}, as well as dependence of γ_λ on T, are due to much smaller contribution of the larger gap to λ_{ab}^{-2} than that to λ_c^{-2}. (iii) γ_λ is close to the calculated ratio of the plasma

TABLE I. Summary of $\lambda_{ab}^{-2}(T)$ and $\lambda_c(T)^{-2}$ study of SrFe$_{1.75}$Co$_{0.25}$As$_2$ (see text for details).

Model	T_c (K)	$\lambda_{ab}(0)$ (nm)	$\lambda_c(0)$ (nm)	ω_{ab}	ω_c	$\frac{2\Delta_{0,1}}{k_B T_c}$	$\frac{2\Delta_{0,2}}{k_B T_c}$
Clean	13.35	315	870	0.04	0.29	7.2	2.7
Dirty	13.30	316	870	0.05	0.35	5.8	1.9

frequencies $\gamma_{\omega_p} = \omega_p^a/\omega_p^c \simeq 2.8$ of $Sr_2Fe_2As_2$ [15]. Bearing in mind that within the London model λ^{-2} is proportional to the superfluid density $\lambda^{-2} \propto n_s/m^*$ (n_s is the charge carrier concentration, m^* is the supercarrier mass). γ_λ can be associated with the anisotropy of the supercarrier mass as $\gamma_\lambda = \gamma_{\omega_p} = m_c^*/m_{ab}^*$. (iv) The gap to T_c ratios are well within the ranges for the big $2\Delta_{0,1}/k_B T_c = 7 \pm 2$ and the small $2\Delta_{0,2}/k_B T_c 2.5 \pm 1.5$ gaps deduced by Evtushinsky *et al.* [28] for Fe-based HTS.

In Fig. 3(b) we plot the difference between the internal magnetic field $\langle B \rangle$ and that measured in the normal state at $T \simeq 20$ K ($\langle B \rangle^{ns}$). In contrast to what is expected for a superconductor, $\langle B \rangle$ *increases* with decreasing temperature. We may clearly rule out the possibility to explain the positive field shift by a paramagnetic Meissner effect, since both ZFC and FC magnetization measurements result in a diamagnetic shift (see Fig. 1). Also, it cannot be explained by the reduction of a hypothetical negative muon Knight shift due to condensation of the carriers into Cooper pairs [29], otherwise the difference between $\langle B \rangle(1.6$ K$)$, measured deeply in the superconducting state, and $\langle B \rangle^{ns}$ would increase with increasing field. The inset in Fig. 3(b) shows, in contrast, that $\langle B \rangle(1.6$ K$) - \langle B \rangle^{ns}$ decreases.

Both, the temperature and the magnetic field dependence of $\langle B \rangle - \langle B \rangle^{ns}$ resemble the situation in the electron doped cuprate HTS $Pr_{2-x}Ce_xCuO_{4-y}$ [11] and $Pr_{1-x}LaCe_xCuO_{4-y}$ [12]. Those reports are different in some details, but agreed that the paramagnetic response in the superconducting state, seen by muons, is caused by the field-induced weak AFM order. The external field applied in c direction leads to the appearance of an additional field component at the muon stopping site, which is *perpendicular* to the c axis [11,12]. We may assume that the paramagnetic response of SFCA, seen in Fig. 3(b), is caused by the same mechanism. The solid line in the inset of Fig. 3(b) corresponds to the fit by $\langle B \rangle(1.6$ K$) = [(\langle B \rangle^{ns})^2 + (B^\perp)^2]^{1/2}$ [11] with the induced field component $B^\perp = 5.2$ mT. We emphasize, that the field-induced AFM order in SFCA is different from that of the parent compound $SrFe_2As_2$, where the magnetic field on the muon site is *parallel* to the c axis [30].

The strong influence of the superconducting phase is observed at an external field as low as 10 mT, which corresponds to the intervortex distance ~ 500 nm. Considering that most of the implanted muons probe the sample outside of the vortex cores, we may conclude that the field-induced AFM order extends throughout the whole sample volume. Further experimental and theoretical studies are needed in order to elucidate the origin of these effects.

To conclude, μSR measurements were performed on a single-crystalline sample of $SrFe_{1.75}Co_{0.25}As_2$ ($T_c \simeq$ 13.3 K). In zero field, superconductivity coexists with dilute Fe moments which are static on the μSR time scale. The mean internal field in the superconducting state in-creases with decreasing temperature, just opposite to the diamagnetic response seen in magnetization experiments. This may be due to weak field-induced antiferromagnetic order leading to appearance of an in-plane magnetic field component on the muon stoping site. The fact that the magnetism is induced by a field as low as 10 mT points to strong interplay between the magnetic and the super-conducting order parameters in Fe-based HTS.

*Corresponding author: rustem.khasanov@psi.ch
[1] S. Wakimoto *et al.*, Phys. Rev. B **63**, 172501 (2001).
[2] M. H. Julien *et al.*, Phys. Rev. Lett. **83**, 604 (1999).
[3] Ch. Niedermayer *et al.*, Phys. Rev. Lett. **80**, 3843 (1998).
[4] S. Sanna *et al.*, Phys. Rev. Lett. **93**, 207001 (2004).
[5] H. Luetkens *et al.*, Nature Mater. **8**, 305 (2009).
[6] J. Zhao *et al.*, Nature Mater. **7**, 953 (2008).
[7] M. Rotter *et al.*, Angew. Chem., Int. Ed. **47**, 7949 (2008).
[8] T. Goko *et al.*, Phys. Rev. B **80**, 024508 (2009).
[9] A. J. Drew *et al.*, Nature Mater. **8**, 310 (2009).
[10] S. Sanna *et al.*, arXiv:0902.215.
[11] J. E. Sonier *et al.*, Phys. Rev. Lett. **91**, 147002 (2003).
[12] R. Kadono *et al.*, J. Phys. Soc. Jpn. **73**, 2944 (2004); R. Kadono *et al.*, J. Phys. Soc. Jpn. **74**, 2806 (2005).
[13] H. Luetkens *et al.*, Phys. Rev. Lett. **101**, 097009 (2008).
[14] F. L. Pratt *et al.*, Phys. Rev. B **79**, 052508 (2009).
[15] D. Kasinathan *et al.*, New J. Phys. **11**, 025023 (2009).
[16] A. Leithe-Jasper *et al.*, Phys. Rev. Lett. **101**, 207004 (2008).
[17] R. Khasanov *et al.*, Phys. Rev. B **78**, 220510(R) (2008).
[18] A. Yaouanc, P. Dalmas de Reotier, and E. H. Brandt, Phys. Rev. B **55**, 11107 (1997).
[19] S. L. Thiemann, Z. Radovic, and V. G. Kogan, Phys. Rev. B **39**, 11406 (1989).
[20] A. Maisuradze *et al.*, J. Phys. Condens. Matter **21**, 075701 (2009).
[21] The zero-temperature values of $\xi_{ab}(0) \simeq \xi_c(0) \simeq 3.4$ nm, estimated from $B_{c2}^{\|c}(0) \simeq 25$ T (see the inset in Fig. 15, Ref. [15]) and accounting for $B_{c2}^{\|c}(0) \simeq B_{c2}^{\perp c}(0)$ [S. A. Baily *et al.*, Phys. Rev. Lett. **102**, 117004 (2009)], result in $\kappa_{ab} = (\lambda_{ab}\lambda_c/\xi_{ab}\xi_c)^{0.5} \sim 130$ and $\kappa_c = \lambda_{ab}/\xi_{ab} \sim 80$, thus confirming the validity of our approach.
[22] R. Khasanov *et al.*, Phys. Rev. Lett. **102**, 187005 (2009).
[23] A. Carrington and F. Manzano, Physica C (Amsterdam) **385**, 205 (2003).
[24] R. Khasanov *et al.*, Phys. Rev. B **77**, 184512 (2008); R. Khasanov *et al.*, Phys. Rev. B **78**, 014502 (2008).
[25] Y. Sekiba *et al.*, New J. Phys. **11**, 025020 (2009).
[26] K. Terashima *et al.*, Proc. Natl. Acad. Sci. U.S.A. **106**, 7330 (2009).
[27] S. Weyeneth *et al.*, J. Supercond. Novel Magnetism **22**, 347 (2009); M. A. Tanatar *et al.*, Phys. Rev. B **79**, 094507 (2009).
[28] D. V. Evtushinsky *et al.*, New J. Phys. **11**, 055069 (2009).
[29] R. Feyerherm *et al.*, Phys. Rev. Lett. **73**, 1849 (1994).
[30] Luetkens *et al.* (to be published).